Seismic performance of 1/4-scale RC frames subjected to axial and cyclic reversed lateral loads

Hakim Bechtoula[†], Masanobu Sakashita[‡], Susumu Kono[‡†], and Fumio Watanabe[‡‡]

Kyoto University, Dept. of Architecture and Architectural Engineering, Sakyo-ku, 606-8501, Japan

Abstract. This paper summarizes an experimental study on the seismic behavior of lower stories of a mid-rise reinforced concrete frame building. Two reinforced concrete frames with two stories and one span were tested and each frame represents lower two stories of an 11-story RC frame building. Both frames were designed in accordance with Japanese design guidelines and were identical except in the variation of axial force. The tests demonstrated that the overall load-displacement relations of the two frames were nearly the same and the first-story column shear was closely related to the column axial load. The columns and beams elongated during both of the tests, with the second-floor beam elongation exceeding 1.5% of the beam clear span length. The frame with higher axial loads developed more cracks that the frame under moderate axial load.

Keywords: reinforced concrete; frame; load cell; plastic hinge; crack; buckling; damage.

1. Introduction

Numerous researchers have performed cyclic tests on isolated reinforced concrete columns, (Bechtoula, *et al.* 2001), (Kono, *et al.* 2002), (Thomsen, *et al.* 1994), (Ang, *et al.* 1989), (Berry, *et al.* 2004). Far fewer tests, (Fenwick, *et al.* 1993), (Sakata, *et al.* 1992), have been performed on statically indeterminate, multi-story, reinforced concrete frames. Such tests are needed to experimentally evaluate the complex interaction among columns, beams and joints during cyclic loading, which can lead to beam growth and to variations in the distribution of column shears in a building.

It is very important to control the residual column elongation or shortening as well as the residual beam elongation after an earthquake for a retrofitting point of view. Indeed, excessive column and beam shortening/elongation may lead to a permanent deformation that may become an obstacle for building serviceability, or in an extreme case may lead to building demolition. Also, the experimental model must be as close as possible to the prototype in order to reflect its real performance during an eventual seismic loading. Hence, the interest of testing an entire frame structure in order to investigate the above selected targets. Two reinforced concrete frames with two stories and one span were designed and tested at Kyoto University to investigate the seismic

† Ph. D. Candidate, E-mail: rc.hakim@archi.kyoto-u.ac.jp
‡ Ph. D. Candidate, E-mail: rc.sakashita@archi.kyoto-u.ac.jp
‡† Associate Professor, E-mail: kono@archi.kyoto-u.ac.jp
‡‡ Professor, E-mail: nabe@archi.kyoto-u.ac.jp

behavior of the lower part of an entire frame shown in Fig. 1. These frames were scaled to 1/4 in order to fit the loading system. The reinforced concrete frames were designed in accordance with the 1999 Japanese guidelines (Design guidelines 1999). The models represented the lower part of an eleven story reinforced concrete frame building prototype. The targets of our tests were to 1) Quantification of bending moment, axial load and shear force distributions in the first story columns, 2) Measure elongation and shortening of the beams and columns, 3) Compare the axial mean strain of the first story columns with those of cantilever columns tested previously, 4) Predict the load-displacement relationships at each story as well as the component deformation analytically and 5) Predict the progression of damage in the columns and beams.
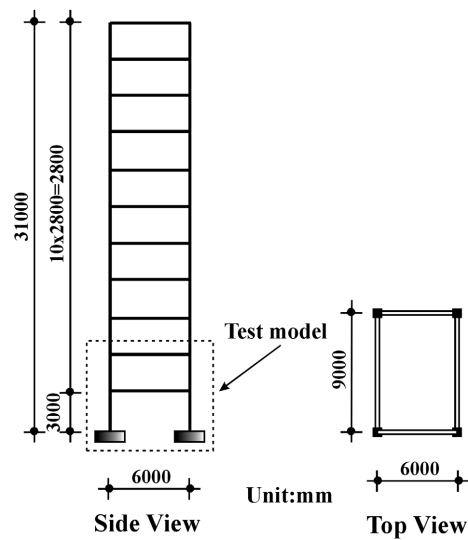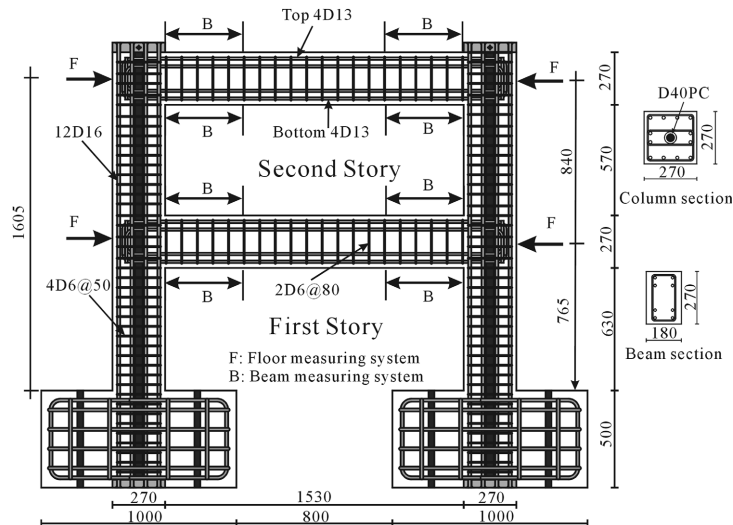

Fig. 1 Prototype building

Fig. 2 Frame dimension and steel arrangement -Model-

2. Experimental program

2.1. Test setup

Fig. 2 shows an elevation of test frames. The heights of the first and second floors were 765 mm and 840 mm respectively, and the span length between the column centers was 1800 mm. The column cross-section measured 270×270 mm and the beam cross-section measured 180×270 mm. Concrete and steel characteristics as well as the test variable are shown in Table 1. The horizontal load was applied through a 1000 kN hydraulic jack at an elevation corresponding to mid-height of the third story, which was 2025 mm high. To distribute the horizontal load evenly to the columns, a 500 kN hydraulic jack was set between the top columns as shown in Fig. 3.

A 45 mm diameter prestressing steel (PS) bars passing through the column centers were used to simulate the axial load effect of the upper stories. The PS bars were used to apply either compression or tension to the columns by means of two jacks, one of which is a center-hole jack, set at the top of each column. During the test, the axial load in the columns, N, was varied linearly with respect to the applied horizontal load, Q. Axial load in columns varied following Eq. (1).

Table 1 Materials characteristics

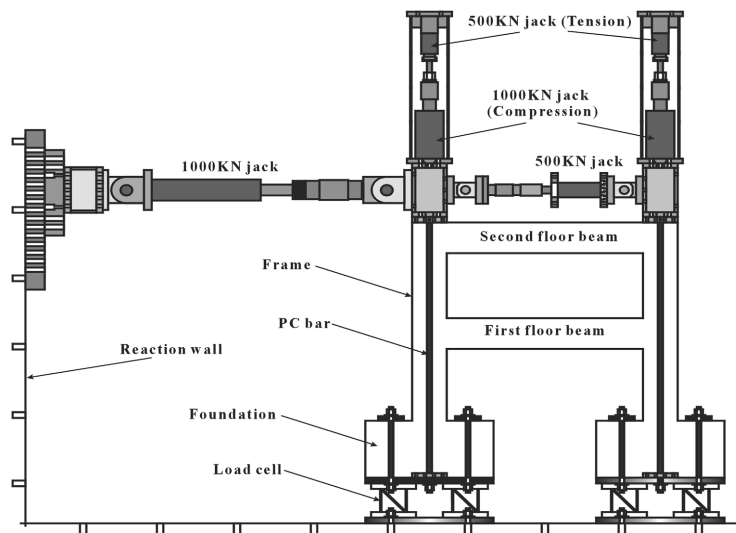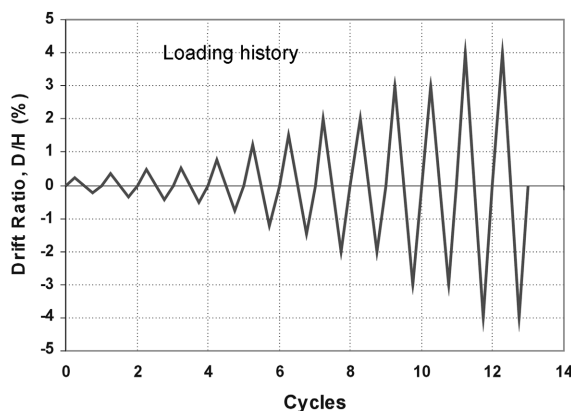| Frame designation	Material			Test variable -Axial load-	
	concrete strength	Longitudinal steel	Transverse steel	Compression $N/f_c' A_g$	Tension $N/f_c' A_g$
SN30	Before 30.47 MPa after 32.07 MPa	Column 12D16 (3.27%) Fy = 346 MPa Beam 8D13 (2.08%) Fy = 332 MPa	Column 4D6@50 (0.94%) Fy = 346 MPa Beam 2D6@80 (0.44%) Fy = 394 MPa	0.3	0.1
SN50				0.5	0.2

Fig. 3 Loading system

Fig. 4 Loading history

$$N = 239 \pm \psi Q(\text{kN}) \qquad (1)$$

The value 239(kN) represented the axial load due to live and dead loads of the upper stories. The ψ value was 3.06 for frame SN30 and 6.12 for frame SN50. Axial load variation in frame SN30 simulated a frame receiving a unidirectional seismic load whereas, that in frame SN50 simulated the axial load variation of a frame receiving a bi-directional seismic loads. Both frames were cycled to the following frame drift percentages: ±0.25, ±0.35, ±0.45, ±0.55, ±0.75, ±1.25, ±1.50, ±2.00, ±3.00, ±4.00. Beyond ±1.50%, the frames were loaded with two cycles instead of one for each drift level as shown in Fig. 4.

To evaluate the axial load, shear force and the bending moment at the base of each first-story column, two identical load cell sets were designed and calibrated before the test. The load cells were analyzed under different loading combination. One load cell set was inserted beneath each foundation as shown in Fig. 2.

2.2. Experimental results

The overall experimental load-drift relationship was slightly different between the two frames in term of peak load. SN50 frame showed a lower loading and unloading stiffness than SN30 frame due to the high tension-compression axial load. This can be seen clearly through Fig. 5 where load-drift curve for the entire frame is shown. The tests were terminated due to the lack of enough space between the top jack that applied the axial load to the south column and an existing steel loading frame. The maximum frame drift ratio reached 6.08% for SN30 and 7.09% for SN50. No strength degradation was observed until this amount of drift ratio for both frames.

Using the load cells beneath the foundations and on the PS bars, shear force, axial load and bending moment at the column's base were determined. From Fig. 6 it can be seen that the total shear force was not distributed evenly to the columns. The shear force carried by columns was found to be sensitive to the axial compression force generated in beams as a result of beam elongation. In Fig. 7, axial load variation in the north and south columns at the first story for frame SN50 is shown as an example.

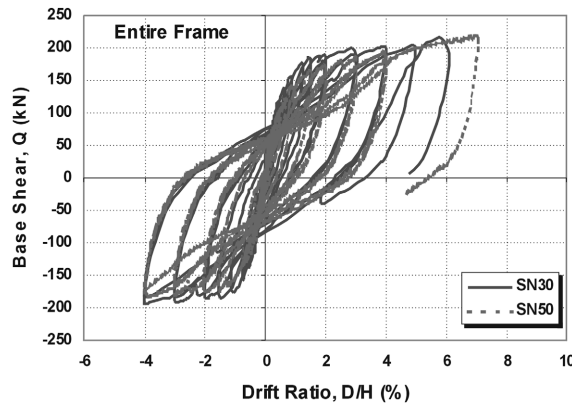Fig. 8 shows the elongation and shortening for the first story columns of frame SN50. The

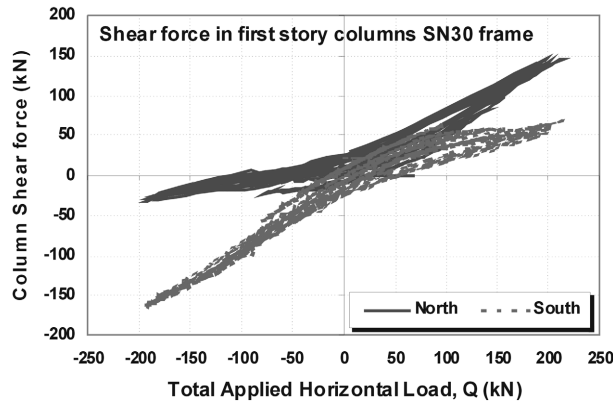Fig. 5 Load displacement relationship
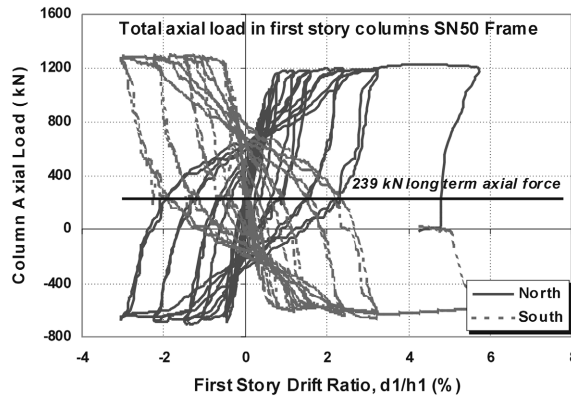

Fig. 6 Shear force at the column bases

Fig. 7 Axial load variation at the column bases SN50 frame

column's shortening were evaluated using the displacement gauges attached in each column. Although the figure is not shown, the first story columns of frame SN30 showed a tendency to elongate rather than shorten especially the column at the south side. The upper two columns showed nearly the same amount of shortening and elongation. The first story columns of SN50 frame
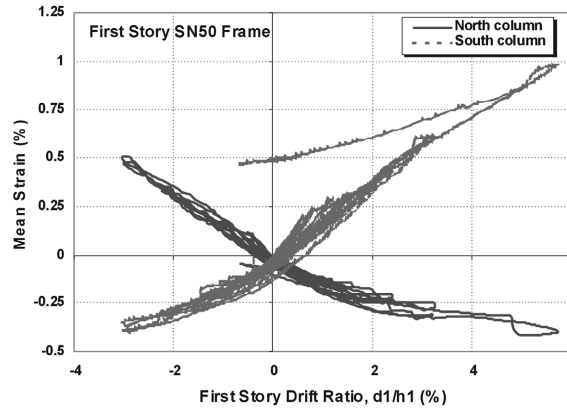
Fig. 8 Mean strain-first story drift relationships for columns of SN50 frame

Table 2 Materials characteristics and test variable for cantilevers columns

Specimen designation	Specimen configuration			Test variables
	Concrete strength f_c' (MPa)	Longitudinal rebar (ratio) [Fy]	Shear rebar (ratio) [Fy]	Slope in normalized moment-axial force relation
D1NVA D1NVB	26.8	12-D13 2,60% 467 MPa	F4@40 0.52% 604 MPa	1.39 2.79

showed nearly the same amount of elongation as for SN30 frame, however the shortening was more important. It can be observed that columns at the first story of both frames followed the same elongation-path while under tension. However, shortening-path was different. Shortening for the south column of SN50 frame was more than two times that observed for SN30 frame.

The first floor column's mean strains were compared to two isolated cantilever columns tested earlier at Kyoto University. The two cantilever columns had the same material properties and geometry configuration as given in Table 2. Axial load varied from zero to $0.6 A_g f_c'$ for both columns. The moment at the column base was varied proportionally to the axial load and their slope on the normalized M-N interaction curve is shown in Table 2.

As illustrated in Fig. 9, first story columns mean strains are much higher than those for cantilever columns, especially for columns under high axial load, SN50 frame. Even though the normalized compression axial load, $N/A_g f_c'$, was 0.5 for specimen SN50 columns and 0.6 for the cantilever columns, the axial strain was more than three times larger as shown in the same figure.

More details concerning the columns and beams elongation and shortening can be found elsewhere (Bechtoula, *et al.* 2004).

2.3. Column curvature-drift angle relationships

Curvature distribution was evaluated at different zones using the displacement gauges attached to columns and beams. Fig. 10 shows the zone identification. Fig. 11 show curvature versus story drift relations at the 4-zones of first-story columns of SN30 frame. At first-story, curvature-drift relation

(a) **First story north column SN50 frame**   (b) **First story south column SN50 frame**
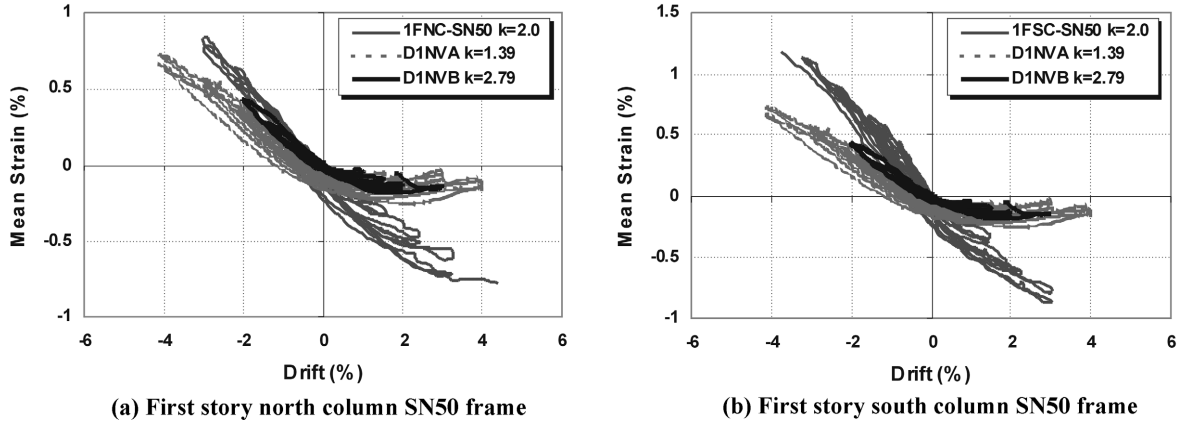
Fig. 9 Comparison between cantilever and first story column's axial strains
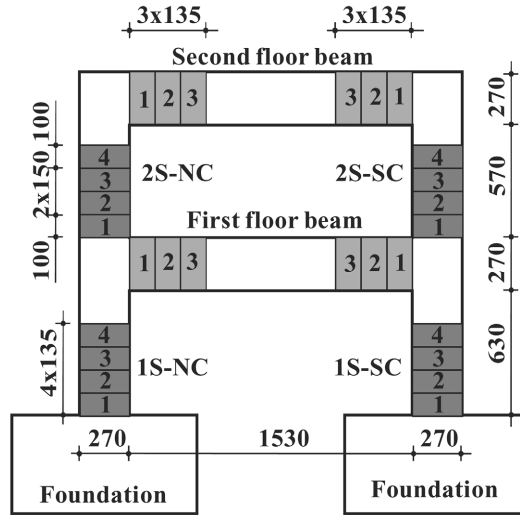

Fig. 10 Zones identification and location

curve tends to move downward for the north column and upward for the south column. This means that at zero drift the first-story columns showed some permanent residual deformation. However, the second-story columns did not show this residual curvature. The same remarks were observed for SN50 frame.

2.4. Variation of equivalent viscous damping

Equivalent viscous damping factor of the first and second loading cycles to each specified displacement was plotted against the drift and shown in Fig. 13. The equivalent viscous damping, h_{eq}, was calculated using the following equation:

$$h_{eq} = \frac{1}{4\pi}\frac{\Delta W}{We}$$ (2)

(a) North column   (b) South column
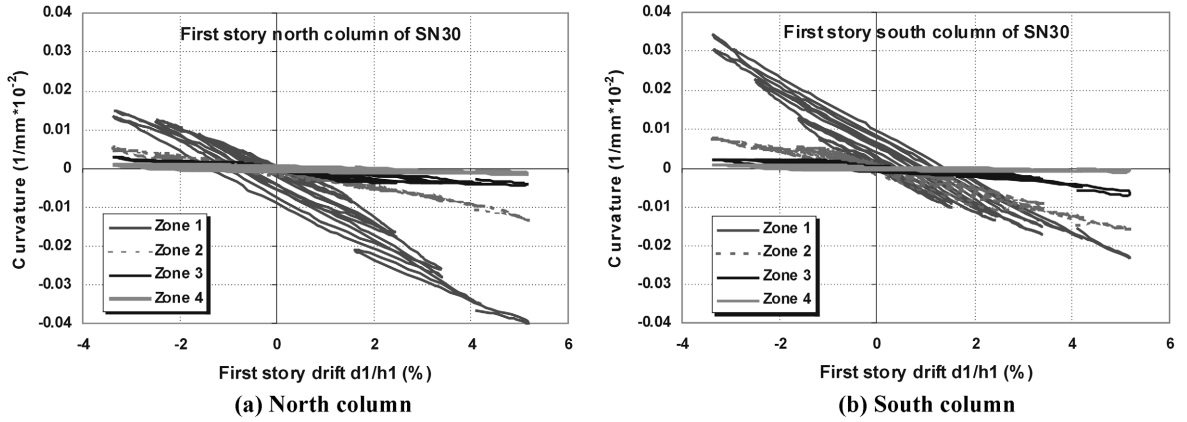
Fig. 11 Curvature distribution at different zones for first-story columns of SN30 frame
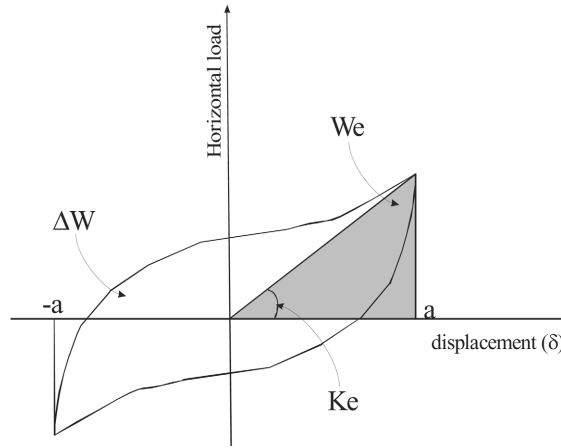

Fig. 12 Definition of equivalent viscous damping

where ΔW is the area enclosed by one cycle of hysteresis loop, and We is the equivalent potential energy represented by the triangle shown in Fig. 12, $We = K_e a^2 / 2$.

Through Fig. 13 it can be seen that the equivalent viscous damping, h_{eq}, increased rapidly for drift-ratio less than 2%. Beyond that limit h_{eq} remains nearly constant around 22%. It can also be observe that, SN50 frame under high axial load, $N / f_c' D^2 = 0.5$, showed lower values of h_{eq} than SN30 frame with a moderate axial load, $N / f_c' D^2 = 0.3$.

2.5. Observed damage and crack distribution

Fig. 14 shows crack patterns at 2% drift angle for small-scale frames. SN50 had more cracks than SN30 by comparing columns. No buckling or severe concrete crushing was found for any column. At the end of the test, spalling of the outside concrete cover located at the base of the first floor column either in the north or south side of the frame was observed, as illustrated in Fig. 15(b). The spalled-height was found to be 26 cm (0.96D) for SN50 and 15 cm (0.56D) for SN30, where "D" is the column depth. Even though the spacing of the shear rebar was as much as 8 cm, six times the
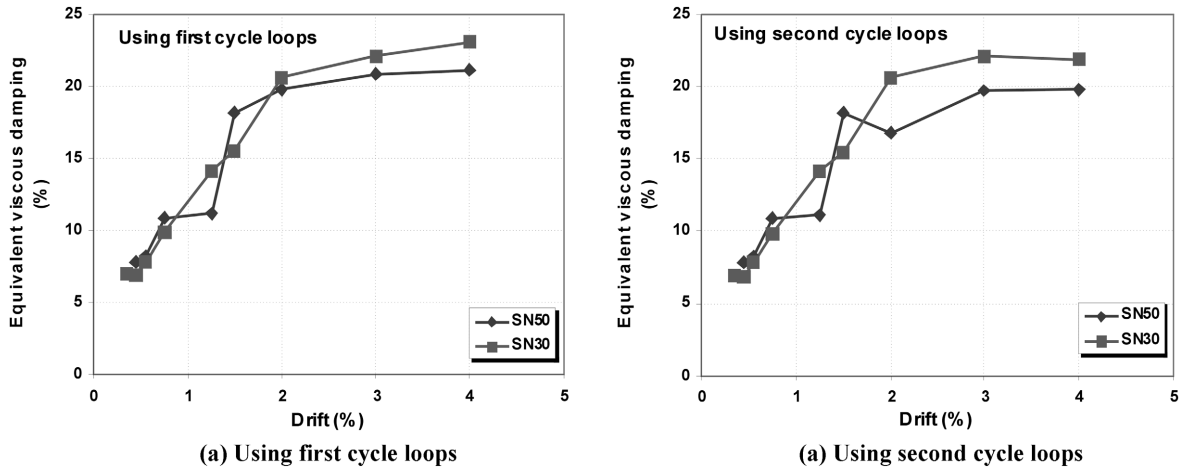
(a) Using first cycle loops   **(a) Using second cycle loops**

Fig. 13 Variation of equivalent viscous damping for small-scale frames

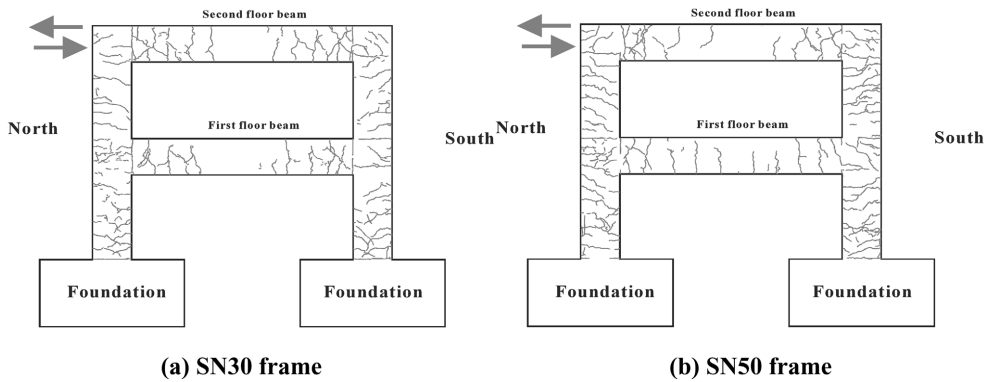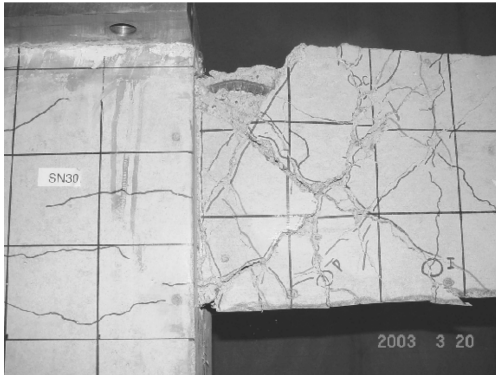**(a) SN30 frame**   **(b) SN50 frame**

Fig. 14 Observed damage

longitudinal bar diameter, buckling of the longitudinal reinforcement of the second floor beam ends were observed for both frames as shown in Fig. 15(a). Concrete of the lower part of the south side of the second floor beam crushed due to high compression, and its length was found to be 10 cm for frame SN30 and 20 cm for frame SN50. The same crushing was found at the upper part of the north side of the second floor beam with 10 cm length for both frames due also to high compression force.

Strain distribution of corner longitudinal reinforcement of the north-column of SN30 frame is compared in Fig. 16. It can be see clearly that strains at external barn, bar 1, are much higher than that of the internal corner bar, bar 4. Fig. 17 shows the location and label of longitudinal reinforcing bars. The large difference in strain distribution is thought to be caused by the high axial, shear and bending moment that the external side of the column is subjected to under positive cyclic loading. However, under negative cyclic loading, the inside of the column bases are subjected to low axial, shear and bending moment. It is worth to mention here that presence of beam axial compression force, as a consequence of beam elongation, is one of the causes that increase/decrease the damage to column bases as illustrated in Fig. 15(b).
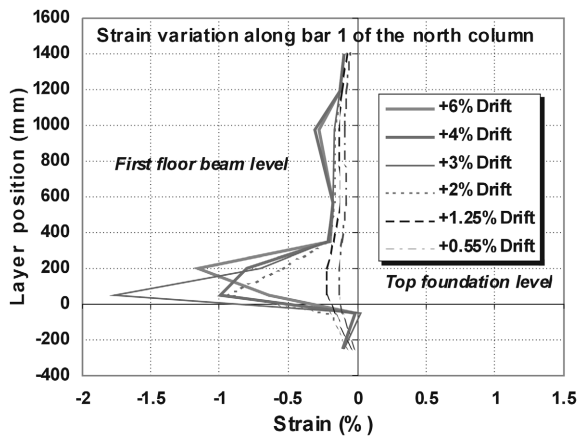
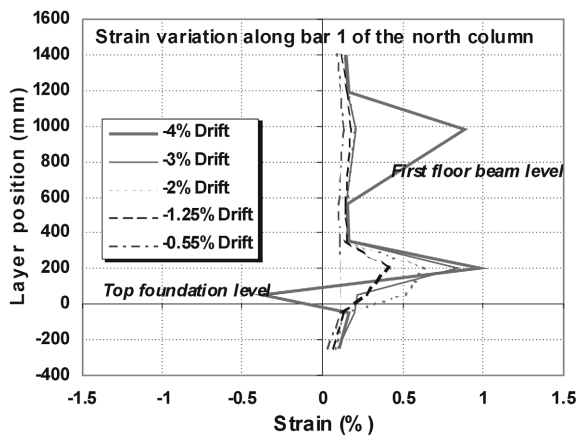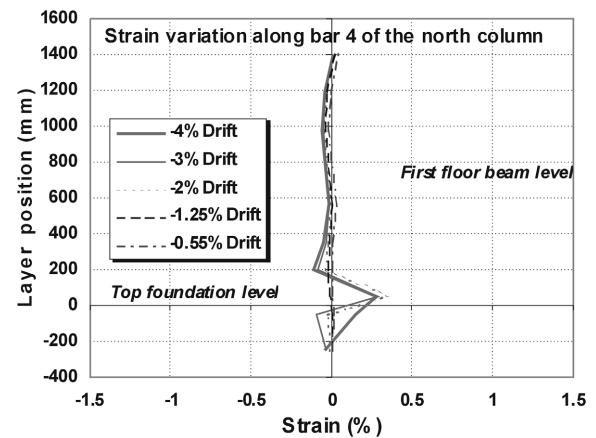**(a) Second floor beam of SN30 frame**   **(b) Spallimg of cover concrete**

Fig. 15 Observed damage at the test end

(a) First case: Bar 1 under positive cycles and bar 4 under negative cycles

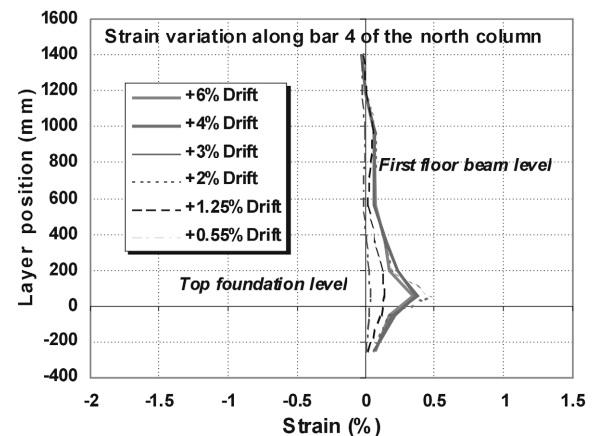**(b) Second case: Bar 1 under negative cycles and bar 4 under positive cycles**

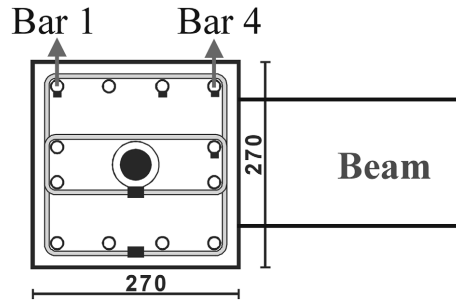Fig. 16 Strain distribution along the longitudinal corner bars height for SN30 frame

Fig. 17 Longitudinal bars identification and location

3. Analytical investigations

3.1. Evaluation of shear force-drift relationships

To predict the envelope curve of the shear force-drift relationship a pushover analysis was carried out using the nonlinear SAP2000 program (Computers and Structures 2002). Columns and beams were modeled with a beam element that exists in the library of the program as shown in Fig. 18(a). Plastic hinges where introduced at each element ends having the characteristics recommended by the Japanese design guidelines (Architecture institute of Japan 1999). A schematic representation of the tri-linear plastic hinge model used for columns is shown in Fig. 19. The pushover analysis is carried out step by step by incrementing the horizontal force until a collapse mechanism is reached. As an example, Fig. 18(b) illustrates the final collapse mechanism of both frames.

In the first trial beams and columns were modeled using the beam-element that exist in SAP2000 library. This trial gave a lower envelope curve compared to the experimental one. The ratios between the analytical to the experimental results, in term of peak load, varied between 84 to 88%. Taking into account the presence of the joint-panel, the accuracy was increased by inserting rigid zones to beam and column ends. The second trial envelope curves were closer to the experimental
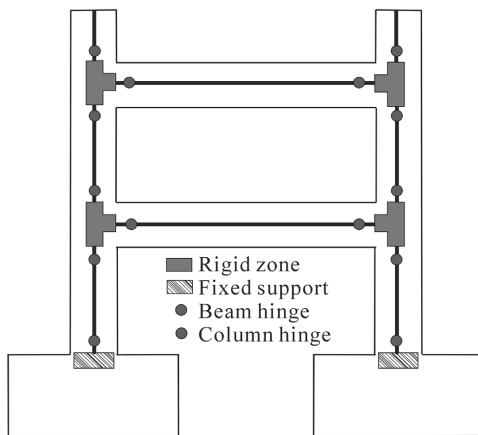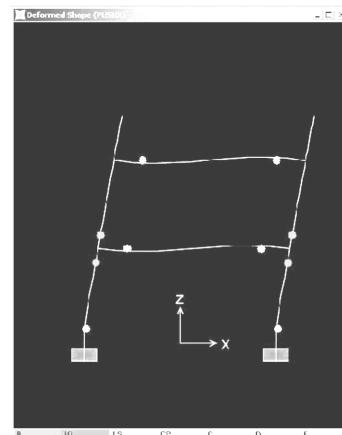
(a) Model   (b) Collapse mechanism of frame SN30

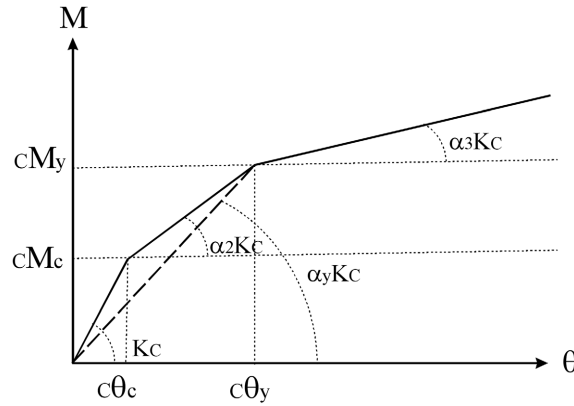Fig. 18 Model and collapse mechanism in SAP2000

Fig. 19 Plastic hinge model for column

Table 3 Comparison between the analytical and experiment maximum peak, Q

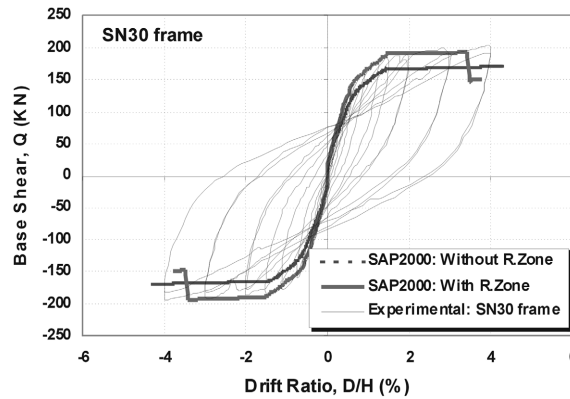| Frame identification	Q-analysis/Q-experimental (Without rigid zone)		Q-analysis/Q-experimental (With rigid zone)	
	Positive	Negative	Positive	Negative
SN30	0.846	0.877	0.963	0.998
SN50	0.838	0.862	0.897	0.923

Fig. 20 Pushover analysis results, SN30

results for both frames. In this case the ratios, defined above, varied between 90 to 100%. A comparison between the experimental and analytical peak load, Q, is given in Table 3. As an example, experimental cyclic loading and analytical envelope curve for SN30 frame is shown in Fig. 20. It is clear that the analytical envelope curves using rigid-zones fit quite well with the experimental hysterisis curves.

3.2. Evaluation of member curvature-drift relationships

The plastic hinge rotation at the end of each member was assessed using SAP2000 and the equivalent plastic hinge length computed using Paulay and Priestley (1992) equation, Eq. (3), was
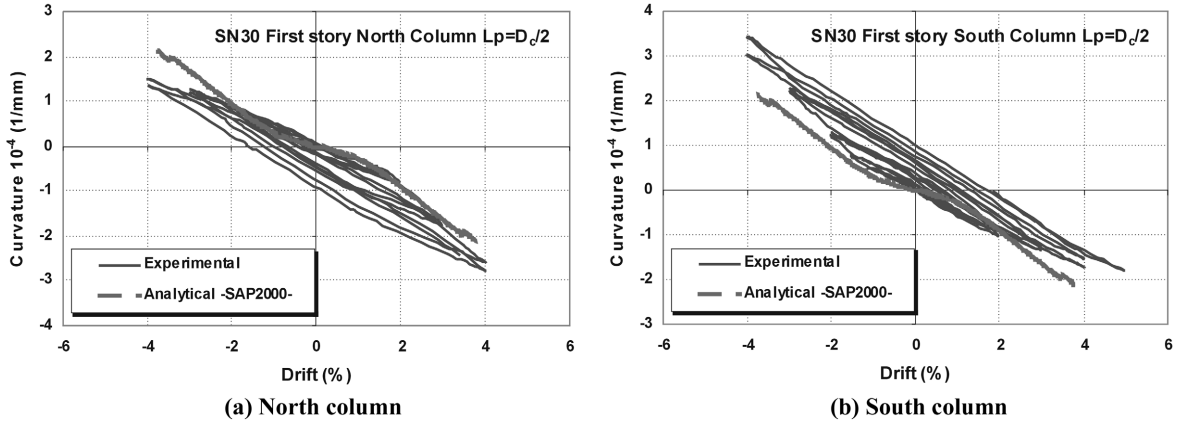
(a) North column

(b) South column

Fig. 21 Analytical and experimental curvature-frame drift relationships at first story column bases of SN30 frame
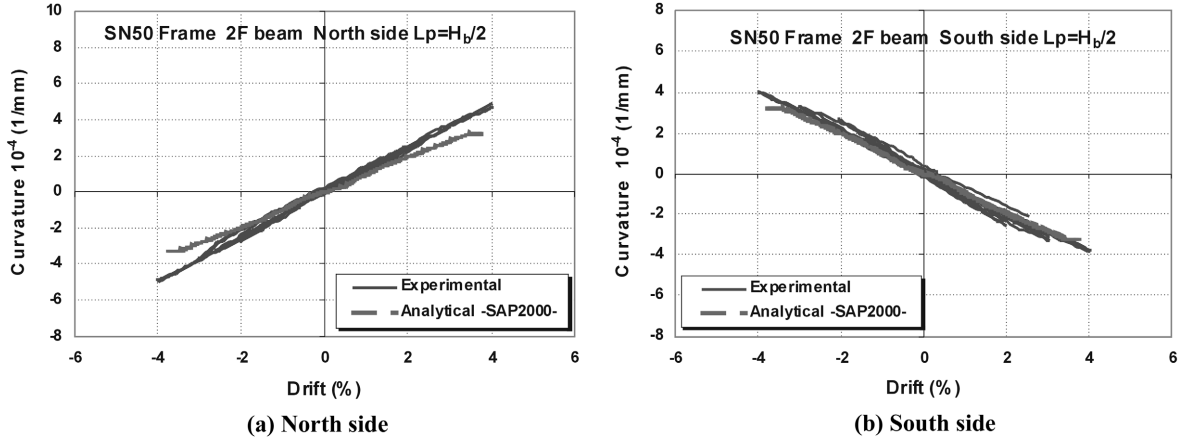

(a) North side

(b) South side

Fig. 22 Analytical and experimental curvature-frame drift relationships at second floor beam ends of SN50 frame

used to compute the curvature at the plastic hinge.

$$L_p = 0.08(M/Q) + 0.022d_b f_y \qquad (3)$$

where, M and Q are the applied bending and shear force, respectively. d_b is the longitudinal bar diameter and f_y is the yielding stress of the bar.

Fig. 21 and Fig. 22 show a comparison between the experimental and the analytical curvature, for some members. A good prediction was observed for both frames either for beams or columns. This method is very simple and can be used as a tool by any engineer to predict the curvature demand at the plastic hinge region for a given probable seismic loadings.

3.3. Evaluation of cracks width

A few reliable crack models exist in the literature. Recently Hyo-Gyoung Kwak, *et al.* (2004) proposed a numerical model for simulating the nonlinear response of RC shear wall subjected to

cyclic loadings. A simple hysteretic rules defining the cyclic stress-strain relations of concrete and steel were designed on the basis of the theoretical background for the shear dominant structural behavior. In our case, crack width variation at beams was predicted for both frames using the Japanese PRC recommendation (Architecture Institute of Japan 1986), crack width variation at beams was predicted for both frames. The average crack width is defined as given in Eq. (4)

$$w_{av} = l_{av}\varepsilon_{t.av} \tag{4}$$

where, l_{av} are $\varepsilon_{t.av}$ the crack spacing and the strain at tensile bar respectively. The crack spacing is computed as:

$$l_{av} = 2(c + s / 10) + \kappa\phi / p_e \tag{5}$$

where:
  $\kappa = 1$ for a beam.
  $\kappa = 0.0025t$ for a slab with thickness t.
  $c = (c_s + c_b)/2$ is the average of the concrete cover.
  s : is the horizontal distance between the tensile bars.
  ϕ : is the bar diameter.
  $p_e = a_t/A_{ce}$ is the ratio of the tensile reinforcement area a_t to the surrounded area A_{ce}.
  $A_{ce} = (2c_b + \phi)b$ with b is the beam width.

Fig. 23 shows the definitions of some of the geometric parameters that were used in Eq. (5). The average tensile strain is computed as:

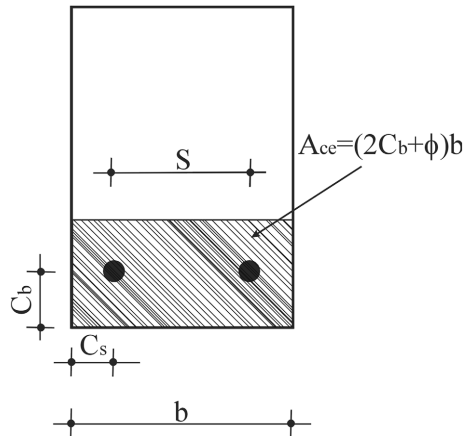$$\varepsilon_{t.av} = \frac{1}{E_s}\left(\sigma_t - \kappa_1\kappa_2\frac{F_t}{p_e}\right) \tag{6}$$

where,

Fig. 23 Definition of some of the used parameter

$$\kappa_1 \kappa_2 \ = \ 1 \ / \ (2.10^3 \, \varepsilon_{t.av} + 0.8) \tag{7}$$

E_s and σ_t are the Young modulus and the tensile stress of the steel bar, respectively. F_t is the concrete tensile strength.

Substituting the value of $\kappa_1 \kappa_2$ given in Eq. (7) into Eq. (6), the final formulation governing the average tensile steel strain is:

$$\varepsilon_{t.av} \ = \ \frac{(2.10^3 \sigma_t - 0.8 E_s) + \sqrt{(2.10^3 \sigma_t - 0.8 E_s)^2 - 8.10^3 E_s (F_t / p_e - 0.8 \sigma_t)}}{4.10^3 E_s} \tag{8}$$

The value of $\varepsilon_{t.av}$ must meet the conditions given in Eq. (9).

$$\varepsilon_{t.av} \geq 0.4 \, \sigma_t / E_s$$

$$\varepsilon_{t.av} \geq (\sigma_t - 1050) / E_s \tag{9}$$

It is worth to mention here that, kilogram (kg) and centimeter (cm) must be used while using the PRC recommendations.

The main problem of the PRC recommendations is the assessment of the steel tensile stress σ_t. However, by combining the section analysis results and the nonlinear SAP2000 program results, the problem was solved easily. Fig. 24 shows the chart that summarizes the different steps used to compute the crack widths.
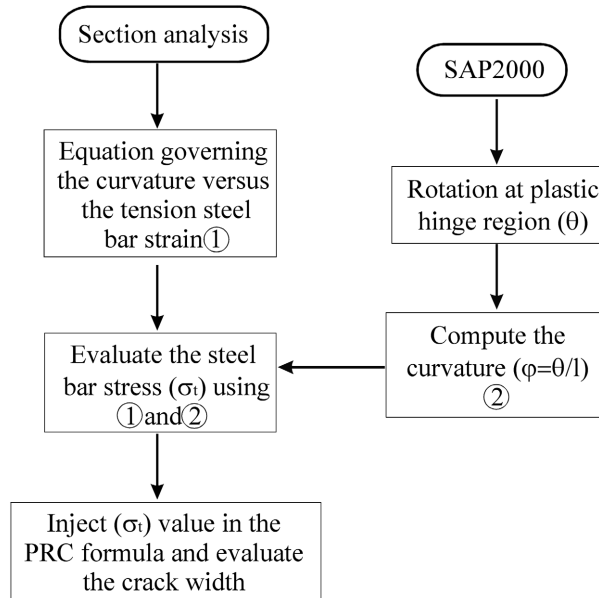

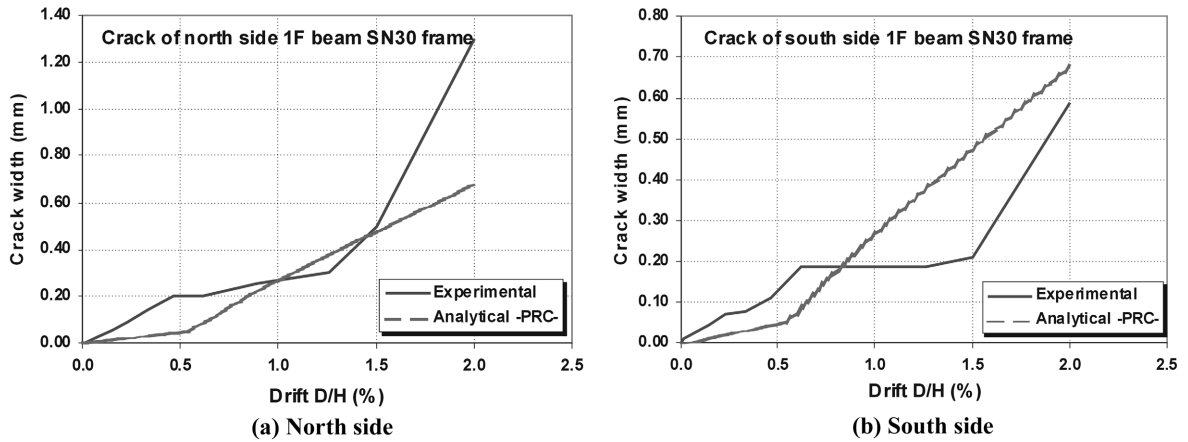Fig. 24 Analytical computation of crack width chart

(a) North side

(b) South side

Fig. 25 Experimental and analytical crack widths of the 1F beam of SN30 frame

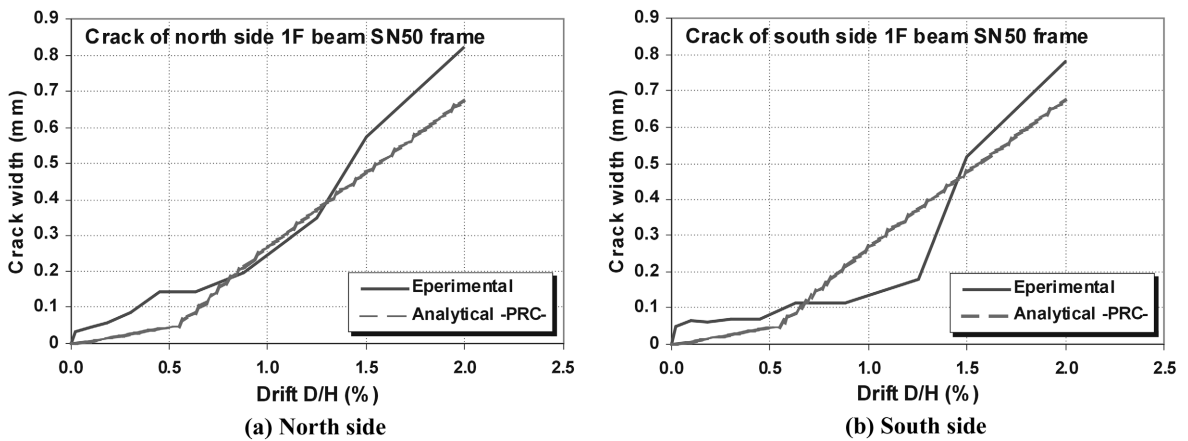

(a) North side

(b) South side

Fig. 26 Experimental and analytical crack widths of the 1F beam of SN50 frame

As an example, Fig. 25 and Fig. 26 show a comparison between the analytical and the experimental crack widths for the first-floor beam of both frames at the north and south side of beam. In general, the average crack width was well predicted until a frame drift of 1.5%, which is quite enough for design purpose.

4. Conclusions

To investigate the seismic performance of the lower part of mid-rise buildings, two 1/4-scale reinforced concrete frames were tested. The following are the main conclusions:
- The total shear force was not distributed evenly among the first-story columns, due to presence of axial load at beams, as a results of beam elongation caused by damage at plastic hinge regions.
- Slight difference between the two frames in term of peak load and the loading and unloading stiffness was observed.

- Cracks, concrete spalling and buckling or reinforcement, was generally localized at beam-ends, near the beam-column joints for a distance equal half of the beam height.
- Concrete spalling was observed only at the external face of the first story columns.
- No serious damage was observed for the second story columns.
- Axial strain for cantilever columns under a higher axial compression was found to be less than that observed at first story columns.
- Equivalent viscous damping decreased with the increased axial load in columns.
- Envelope curves of the lateral load-drift relations were predicted with a good accuracy using the nonlinear SAP2000 program where plastic hinge regions were modeled with the tri-linear model suggested by the Japanese design guidelines.
- Column and beam curvature-drift relationships were successfully predicted for a plastic hinge length equal to half of the column depth and half of the beam height.
- Using the Japanese PRC recommendations, average crack width was quite well predicted with a modified, linear, steel stress-strain relation.

Acknowledgements

References

Ang Beng Ghee, M. J. N. Priestley, and T Pauly (1989), "Seismic shear strength of circular reinforced concrete columns", *ACI Struct. J.*, 45-59.

Architectural Institute of Japan, AIJ, (1986), "Recommendations for design and construction of partially prestressed concrete (Class III of prestressing concrete) structure PRC", (in Japanese).

Architectural Institute of Japan, AIJ, (1999), "Design guidelines for earthquake resistant reinforced concrete buildings based on inelastic concept", (in Japanese).

Bechtoula, H., Arai, Y., Kono, S., Watanabe, F. (2001), "damage assessment of RC columns under large axial and lateral loadings", *Symposium on a Design Procedure of RC Structures Based on Inelastic deformation - Use of confined concrete-*, 263-270.

Bechtoula H., Sakashita M., Kono S., Watanabe F. and Eberhard M. O. (2004), "Experimental and analytical study of 1/4-scale RC-frames subjected to cyclic lateral loads", *International Conference on Concrete under Severe Conditions Environment and Loadings CONSEC'04*, Seoul June 27-30, **2**, 1256-1263.

Berry, M. P., Parrish, M. and Eberhard, M.O. (2004), PEER Structural Performance Database User's Manual, Pacific Earthquake Engineering Research Center Report PEER-2004-, University of California, Berkeley, (in press).

Fenwick, R. C. and Megget, L.M. (1993), "Elongation and load deflection characteristics of reinforced concrete members containing plastic hinges", *Bulletin on the National Society for Earthquake Eng.*, **26(1)**, 28-41.

Kwak, H. G. and Kim, D. Y. (2004), "Cracking behavior of RC shear walls subjected to cyclic loading", *Comput. and Concrete, An. Int. J.*, 1(1), 77-98.

Kono, S., Bechtoula, H., Kaku, T., Watanabe, F. (2002), "Damage assessment of RC columns subjected to axial load and bi-directional bending", *Proceeding of the Japan Concrete Institute*, **24(2)**, 235-240 (in Japanese).

Matthews, J., Bull D., and Mander J. (2001), "Investigating the load paths of floor diaphragm forces during severe damaging earthquakes", *Proceedings of Combined Concrete Society and Ready Mix*, TR24, Rotorua,

122-31.

Paulay, T. and Priestley, M. N. (1992), *Seismic Design of Reinforced Concrete and Masonry Buildings*, New York: John Wiley & Sons.

SAP2000, linear and nonlinear static and dynamic analysis and design of three-dimensional structures (2002), Integrated Finite Elements Analysis and design of structures, A Product of Computer & Structures, Inc., Version 8.0.

Sakata, H. and Wada, A. (1992), "Elasto-plastic behavior of one-twentieth scale RC frame", *Proceedings of the 10th World Conference on Earthquake Eng.*, **6**, Balkema, Rotterdam, 3335-3340.

Thomsen, H. and Wallace, W. (1994), "Lateral load behavior of RC columns constructed using high-strength materials", *ACI Struc. J.*, 605-615.

CC